JACS
JOURNAL OF THE AMERICAN CHEMICAL SOCIETY
Article
Cite This: J. Am. Chem. Soc. 2018, 140, 7176−7186
pubs.acs.org/JACS

Optical Intramolecular Electron Transfer in Opposite Directions through the Same Bridge That Follows Different Pathways

Eric J. Piechota,[†] Ludovic Troian-Gautier,[†] Renato N. Sampaio,[†] M. Kyle Brennaman,[†] Ke Hu,[†] Curtis P. Berlinguette,[‡] and Gerald J. Meyer*[,†]

[†]Department of Chemistry, The University of North Carolina at Chapel Hill, Murray Hall 2202B, Chapel Hill, North Carolina 27599, United States

[‡]Departments of Chemistry and Chemical & Biological Engineering, and the Stewart Blusson Quantum Matter Institute, The University of British Columbia, 2036 Main Mall, Vancouver, British Columbia V6T 1Z1, Canada

Supporting Information

ABSTRACT: The electrochemical and spectroscopic properties of eight bis(tridentate) cyclometalated Ru^{II} compounds covalently linked by a phenyl- or xylyl-thiophene bridge to a pendant triphenylamine (TPA) were characterized in fluid solution and immobilized on metal oxide surfaces. Upon surface immobilization, the $TPA^{+/0}$ reduction potentials of the phenyl-bridged compounds exhibited large changes, ±100 mV, relative to solution-based values, yet those observed for the xylyl-bridged compounds were relatively unchanged. The highest occupied molecular orbital of the surface-immobilized compounds was associated with either TPA or Ru^{II}, enabling the study of the electron transfer in opposite directions. Electron transfer in the mixed-valent states of the compounds was found to proceed by different optical pathways for $Ru^{II} \rightarrow TPA^{+}$ relative to $TPA \rightarrow Ru^{III}$. Mulliken−Hush analysis of intervalence charge transfer bands for the phenyl-bridged compounds revealed that the electronic coupling matrix element, H_{DA}, was ∼950 cm^{-1} for $Ru^{II} \rightarrow TPA^{+}$, while H_{DA} for $TPA \rightarrow Ru^{III}$ appeared to be 2500 cm^{-1}. In contrast, the xylyl-bridged compounds were weakly coupled. A superexchange analysis, where unoccupied bridge orbitals were taken directly into account, led to a very different conclusion: H_{DA} did not depend on the charge-transfer direction or path. The results imply that the electron-transfer direction can alter optical charge transfer pathways without influencing the electronic coupling.

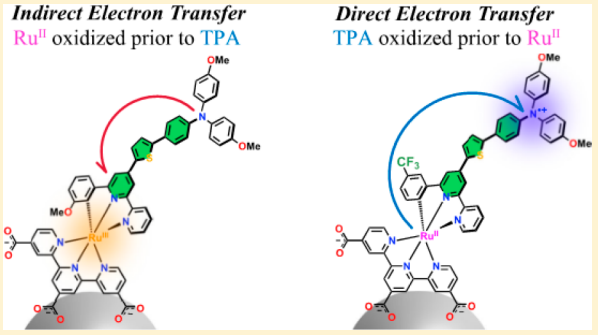

INTRODUCTION

Covalently linked donor−bridge−acceptor compounds composed of bimetallic, organometallic, or organic redox-active centers have garnered intense interest for application in molecular wires and switches,[1−5] conductive metal−organic frameworks,[6] logic gates,[7,8] information storage,[9] and solar energy conversion.[10−14] In one class of compounds, the bridge contains oligomers of π-electron rich units that allow quantum mechanical mixing (H_{DA}) of the donor and acceptor wave functions. This extended conjugation enhances light absorption and influences the yield and rate of electron transfer.[15,16] Large bodies of theoretical and experimental[10−12] research have focused on how subtle changes in molecular structure control the degree of electronic coupling through substituent effects,[17] geometry,[18,19] or protonation state.[20] Surprisingly little research has investigated how the direction of electron transfer can dictate the discrete molecular orbitals, i.e., an orbital pathway, that participate in moving the electron between a donor and an acceptor.[21,22] Here, we report systematic studies of this type showing that different pathways are accessed depending on the direction of optical electron transfer through a common bridge.

Investigating directional thermal and optical electron transfer is both fundamentally meaningful and practically important. Indeed, for solar energy conversion it is often desirable to translate charge toward a catalytic site or to prevent unwanted thermal recombination reactions. Natural and artificial photosynthesis achieve this charge separation through free energy gradients of spatially arranged redox-active centers.[23] In a similar way, for solar energy conversion and storage, light excitation of Ru^{II} polypyridyl compound results in electron injection into TiO_2 and formation of Ru^{III}. Subsequently, a covalently bound electron donor reduces the Ru^{III} and effectively relocates the hole away from the TiO_2 surface. In principle, the bridge would facilitate the charge separation and inhibit unwanted reverse reactions made possible through coupling of the two redox sites. As such, a systematic study where the direction of electron transfer was reversed around an identical molecular bridge presents a fundamentally important contribution to the literature.

Such an experimental approach is depicted in Scheme 1. Two Ru^{II} compounds covalently linked to a pendant triphenylamine (TPA), the structures of which are described further below, are immobilized onto metal oxide thin films. Through careful

Received: March 9, 2018
Published: May 7, 2018

DOI: 10.1021/jacs.8b02715
J. Am. Chem. Soc. 2018, 140, 7176−7186

Scheme 1. Representation of the Reversal of the Electron-Transfer Pathway Following One-Electron Oxidation

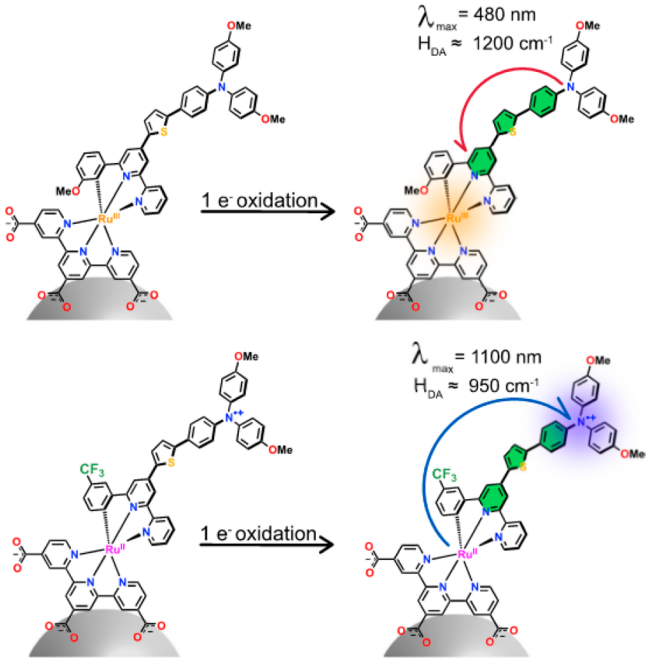

synthetic modification, the highest occupied molecular orbital (HOMO) is varied between the two compounds, either being localized onto the Ru^{II} or on the TPA moiety. Upon electrochemical oxidation, mixed-valent states are obtained and characterized by markedly different charge-transfer spectroscopic features. These features are indicative of accessing discrete optical pathways that depend on the electron-transfer direction, i.e., which redox center the electron originates from. Experimentally observed spectroscopic features are reminiscent of intervalence charge transfer (IVCT) transitions and provide, through theoretical work by Mulliken and Hush, a direct measurement of H_{DA} through analysis of the IVCT band.[24−27]This analysis indicated very different electronic coupling mechanisms between Ru^{II} and TPA, either "*direct*" Ru^{II}/TPA coupling or "*indirect*" coupling using unoccupied high-energy states, an effect commonly termed superexchange.[28]

This study utilizes eight bis-tridentate cyclometalated Ru^{II} compounds covalently bound to a pendant 4,4′-dimethoxy-substituted TPA through an aryl-thiophene bridge, Chart 1. Substitution on the cyclometalating ring allowed for independent tuning of the $Ru^{III/II}$ reduction potential, with either an electron-donating methoxy group (**1**) or an electron-withdrawing trifluoromethyl group (**2**).[29] The TPA unit was chosen because it provides an independent spectroscopic handle of the redox chemistry and has promising hole-transport properties for energy applications.[30,31] Spectroscopic and electrochemical characterization of the eight compounds indicated that the pendant $TPA^{+/0}$ potential varied minimally across the series.

The choice of bridge, either a phenyl- (**p**) or xylylthiophene (**x**) unit, allowed for independent modification of the electronic coupling by enforcing a rotational energy barrier that tuned orbital overlap.[32] Further, substitution in the *para* position of the pyridines that constitute the terpyridine ligand, either ethyl ester (**E**) or carboxylate (**C**), enabled investigation both in fluid solution and anchored onto conductive thin films of In:SnO_2 nanoparticles (nITO). Surface immobilization of the $\mathbf{1p_C}$ series resulted in a negative shift in the $TPA^{+/0}$ reduction potential relative to the solution value of $\mathbf{1p_E}$ that was absent for all xylyl-bridged compounds.

Chart 1. Nomenclature and Structures of the Eight Compounds Studied

Compound	Substituent			
	R_1	R_2	R_3	R_4
$\mathbf{1p_E}$	-H	$-OCH_3$	-H	$-CH_2CH_3$
$\mathbf{1x_E}$	$-CH_3$	$-OCH_3$	-H	$-CH_2CH_3$
$\mathbf{2p_E}$	-H	-H	$-CF_3$	$-CH_2CH_3$
$\mathbf{2x_E}$	$-CH_3$	-H	$-CF_3$	$-CH_2CH_3$
$\mathbf{1p_C}$	-H	$-OCH_3$	-H	-H
$\mathbf{1x_C}$	$-CH_3$	$-OCH_3$	-H	-H
$\mathbf{2p_C}$	-H	-H	$-CF_3$	-H
$\mathbf{2x_C}$	$-CH_3$	-H	$-CF_3$	-H

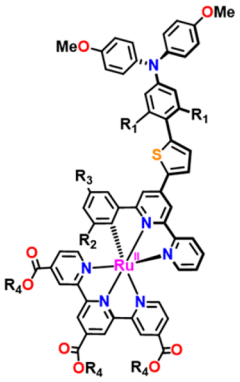

RESULTS

The UV−vis absorption spectrum for the ester and carboxylate compounds in neat acetonitrile and methanol are presented in Figure 1. In all cases, appreciable absorption features extending beyond 700 nm were observed, with no significant absorbance beyond 800 nm.

The extinction coefficients for $\mathbf{1p_E}$ and $\mathbf{2p_E}$ in CH_3CN were similar to those reported previously for the methyl ester derivatives in neat CH_3OH.[33] Absorption features observed between 500 and 600 nm were assigned as typical Ru^{II} metal-to-ligand charge-transfer (MLCT) transitions.[34] The band at 450 nm was assigned to intraligand charge transfer (ILCT) transitions between the cyclometalating ligand and the pendant TPA.[35] We note, however, that the covalent Ru−C bond and C_1-symmetric Ru^{II} center complicates traditional assignment of MLCT and ILCT transitions as the orbital mixing between the ligands and metal is strong.[36] Absorption features below 400 nm correspond to $\pi \rightarrow \pi^*$ transitions of TPA, terpyridine, and the cyclometalating ligand. In general, the extinction coefficients of the **x**-series were found to be lower than that of the **p**-series at wavelengths greater than 400 nm. In the UV region (ca. 330 nm), the **x**-series exhibited higher extinction coefficients, $\varepsilon = \sim 65 \times 10^3\ M^{-1}\ cm^{-1}$, than those measured for the **p**-series, $\varepsilon = \sim 50 \times 10^3\ M^{-1}\ cm^{-1}$. The extinction coefficients and absorption maxima are presented in Table 1.

The $Ru^{III/II}$ and $TPA^{+/0}$ reduction potentials were measured in 0.1 M $LiClO_4/CH_3CN$ for the ester-substituted compounds through spectroelectrochemical methods, Figure 2. Insets showing single-wavelength absorption changes as a function of applied potential illustrate TPA^+ formation and Ru^{II} MLCT disappearance over the potential range. All electrochemical potentials reported here are given vs NHE. For the compounds in fluid solution, the application of positive potentials resulted in spectral changes indicative of two consecutive, one-electron oxidation events through the appearance of isosbestic points. Applying potentials between +800 and +950 mV resulted in the appearance of absorption bands beyond 700 nm, $\lambda_{max} = \sim 750$ nm, indicative of TPA^+ formation which were observed prior to Ru^{II} oxidation events in all cases.[37] For $\mathbf{1p_E}$ and $\mathbf{2p_E}$, bleaches in ground-state absorption were also observed below 700 nm, λ_{max} ~450 and 520 nm. However, growth beyond 800 nm was

DOI: 10.1021/jacs.8b02715
J. Am. Chem. Soc. 2018, 140, 7176−7186

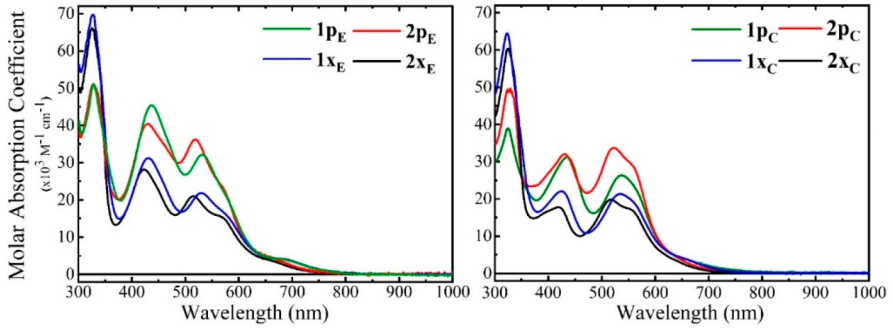

Figure 1. Absorption spectra of the ester forms of the compounds in neat CH_3CN (left). Absorption spectra of the carboxylate forms of the compounds in CH_3OH containing tetrabutylammonium hydroxide (right).

Table 1. Spectroscopic and Electrochemical Properties of the Compounds Studied

		$E_{1/2}$ (mV vs NHE)			
compd	λ_{max} (nm) ($\varepsilon \times 10^3$ M^{-1} cm^{-1})	$Ru^{III/II}$, α	$TPA^{+/0}$, α	ΔE^e (mV)	K_c^f
$\mathbf{1p_E}$[a]	328 (50.5), 437 (45.0), 531 (32.0)	950,[c] 1.10	875,[c] 1.05	75	19
$\mathbf{2p_E}$[a]	327 (50.5), 430 (40.4), 519 (36.0)	1110,[c] 1.15	930,[c] 1.14	180	1100
$\mathbf{1x_E}$[a]	327 (69.0), 431 (31.0), 530 (22.0)	960,[c] 1.17	915,[c] 1.03	45	6
$\mathbf{2x_E}$[a]	325 (65.0), 422 (28.0), 514 (21.0)	1085,[c] 1.05	925,[c] 1.05	160	420
$\mathbf{1p_C}$[b]	325 (39.6), 436 (31.3), 536 (26.7)	865,[d] 1.41	940,[d] 1.16	−75	0.05
$\mathbf{2p_C}$[b]	324 (49.3), 430 (32.0), 522 (33.7)	1050,[d] 1.50	955,[d] 1.15	90	33
$\mathbf{1x_C}$[b]	323 (63.3), 425 (22.0), 535 (21.5)	840,[d] 1.23	920,[d] 1.02	−80	0.04
$\mathbf{2x_C}$[b]	325 (61.0), 418 (17.8), 517 (19.8)	1010,[d] 1.32	945,[d] 1.17	65	13

[a]Recorded in neat CH_3CN. [b]Recorded in CH_3OH with ~1 equiv of TBAOH. [c]Measured in 0.1 M $LiClO_4/CH_3CN$ solution. [d]Measured after being anchored onto nITO in 0.1 M $LiClO_4/CH_3CN$ solution. [e]Calculated relative to $E_{1/2}(TPA^{+/0})$. [f]From eq 3.

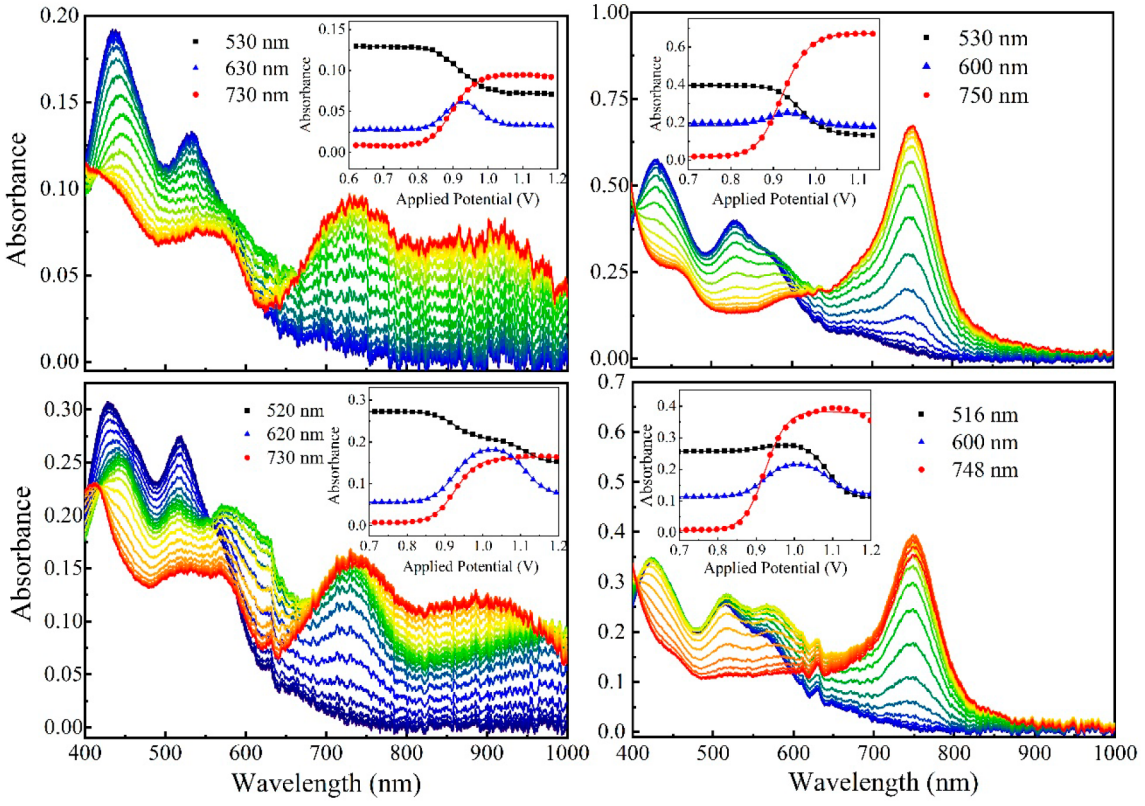

Figure 2. Representative spectroelectrochemical data for $\mathbf{1p_E}$ (upper left), $\mathbf{2p_E}$ (lower left), $\mathbf{1x_E}$ (upper right), and $\mathbf{2x_E}$ (lower right) in CH_3CN containing 0.1 M $LiClO_4$. Insets show single wavelength absorption changes as a function of applied potential, and all applied potentials are reported vs NHE.

DOI: 10.1021/jacs.8b02715
J. Am. Chem. Soc. 2018, 140, 7176−7186

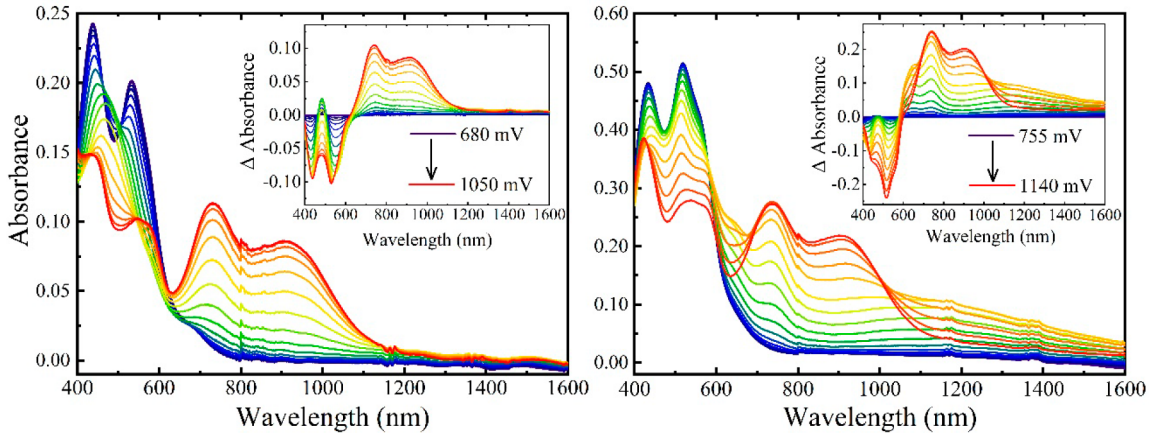

Figure 3. Spectroelectrochemical oxidation of **1p$_C$/nITO** (left) and **2p$_C$/nITO** (right). Insets show difference spectra taken relative to 0 mV of applied potential. Applied potentials are vs NHE.

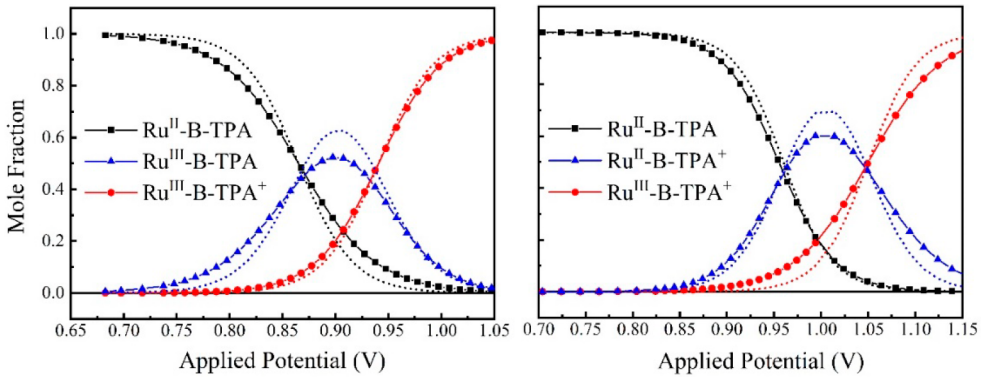

Figure 4. Plots of mole fractions for **1p$_C$/nITO** (left) and **2p$_C$/nITO** (right) in the ground, Ru^{II}–B–TPA (black), doubly oxidized, Ru^{III}–B–TPA$^+$ (red), and one-electron oxidized states (blue), as a function of applied electrochemical potential, where B represents the phenyl-thiophene bridge. The dashed lines represent the mole fractions for ideal (α = 1) Nernstian behavior.

essentially absent in **1x$_E$** and **2x$_E$** within the same range of applied potentials. Applying potentials between +920 mV and +1100 mV resulted in spectral bleaches below 700 nm for **1p$_E$**, **1x$_E$**, **2p$_E$**, and **2x$_E$**, indicative of Ru^{III} formation by the loss of the MLCT transitions.

The carboxylate-derivatized compounds were anchored to mesoporous nITO thin films, and the Ru$^{III/II}$ and TPA$^{+/0}$ formal reduction potentials for **1p$_C$/nITO**, **2p$_C$/nITO**, **1x$_C$/nITO**, and **2x$_C$/nITO** were obtained through UV–vis–NIR spectroelectrochemistry in a similar fashion as described above. Similar solution-phase experiments were not possible for the carboxylate compounds due to limited solubility in CH_3CN. At applied potentials between +750 and +1100 mV, large absorption changes were observed throughout the visible and NIR regions, indicative of multiple redox events that occurred nearly simultaneously. Indeed, in many cases the growth of TPA$^+$ at 750 nm was coincident with the bleach of Ru^{II} at ~500 nm. Upon application of potentials beyond +1150 mV vs NHE, the TPA$^+$ feature was observed to decrease, which indicated an additional oxidation event, presumably the second oxidation of the TPA moiety. Representative spectroelectrochemical data is shown in Figure 3 for **1p$_C$** (left) and **2p$_C$** (right). The corresponding data for **1x$_C$** and **2x$_C$** in the mixed-valent state did not show appreciable absorption features indicative of electronic coupling, as presented in the Supporting Information (SI). The reduction potentials, non-ideality factors, and electrochemical splitting are given in Table 1.

Formal reduction potentials were measured when equal concentrations of the reduced, [Red], and oxidized, [Ox], species were present. A modified Nernst equation was used to model changes in absorbance at single wavelengths corresponding to each redox event, eq 1, where R is the gas constant and F is Faraday's constant.[38] In all cases, a non-ideality factor, α, was necessary to model the spectroelectrochemical data, $\alpha > 1$.

$$E = E_{1/2} - \frac{\alpha RT}{nF} \ln\left(\frac{[\text{Red}]}{[\text{Ox}]}\right) \quad (1)$$

In all cases, α was larger for compounds immobilized on nITO compared to the solution counterparts. Such non-ideality represents deviations from Nernstian 59 mV steps to acheve a factor of 10 change in concentration, as discussed later. However, in general, the modeled changes in TPA$^{+/0}$ absorption features were more Nernstian than was the Ru$^{III/II}$ redox chemistry.[39]

Accurate modeling of the IVCT bands was difficult due to overlapping absorption features, small difference between Ru$^{III/II}$ and TPA$^{+/0}$ reduction potentials, $\Delta E \sim 80$ mV, and non-ideal electrochemistry. A small electrochemical window existed where appreciable concentrations of the mixed-valent forms were spectroscopically detectable, as predicted by the comproportionation constants, K_c, in Table 1 and defined in eq 2a.[40,41] In essence, K_c describes the relative thermodynamic stabilization of the one-electron oxidized mixed-valent state

DOI: 10.1021/jacs.8b02715
J. Am. Chem. Soc. 2018, 140, 7176–7186

relative to the ground state and doubly oxidized state of the compounds, eq 2b.

$$K_c = \exp\left(\frac{nF}{RT}\Delta E\right) \quad (2a)$$

$$Ru^{II}-B-TPA + Ru^{III}-B-TPA^{+} \rightleftharpoons 2Ru^{II}-B-TPA^{+} \quad (2b)$$

Figure 4 shows the mole fractions of the ground state and the singly and doubly oxidized states as a function of applied potential. Without comproportionation corrections, the concentration of the mixed-valent state would be underestimated on the basis of the assumption that all of the molecules were in a one-electron oxidized state. For example, before comproportionation corrections, the extinction coefficient for the IVCT band in **2p$_C$/nITO** was found to be $\varepsilon_{max} = 7.5 \times 10^3$ M^{-1} cm^{-1}, yet increased by nearly 45% to $\varepsilon_{max} = 10.8 \times 10^3$ M^{-1} cm^{-1} after accounting for the true mixed-valent compound concentration due to comproportionation and non-Nernstian electrochemistry. This is evident in Figure 4 as the mixed-valent state (blue triangles) represents only 50% of the total number of molecules on the surface. This analysis also revealed that the transition observed at 480 nm had a larger extinction coefficient after correction, $\varepsilon_{max} = 29.8 \times 10^3$ M^{-1} cm^{-1}, than the value, $\varepsilon_{max} = 25 \times 10^3$ M^{-1} cm^{-1}, initially measured from the uncorrected spectra. Figure 5 shows the experimentally observed spectra for **1p$_C$/nITO** and **2p$_C$/nITO** after one-electron oxidation, as well as the spectrum corrected for comproportionation chemistry.

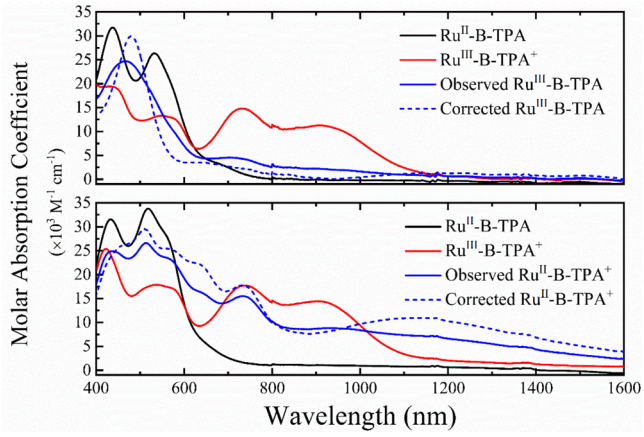

Figure 5. Absorption spectra of **1p$_C$/nITO** (top) and **2p$_C$/nITO** (bottom) in their ground (black), one-electron oxidized (blue), and two-electron oxidized (red) states. The dashed blue line represents the comproportionation correction in the mixed-valent state from spectral modeling which reveals intense IVCT-type transitions at 450 nm for **1p$_C$/nITO** and 1100 nm for **2p$_C$/nITO**.

DISCUSSION

The ground state and one- and two-electron oxidized states of eight donor–acceptor compounds of the type Ru^{II}–B–TPA with a phenyl- or xylyl- bridge were characterized in fluid solution and anchored to metal oxide thin films, Figures 2 and 3. These compounds were previously used for applications in dye-sensitized solar cells: the MLCT excited states quantitatively injected electrons into TiO_2 and subsequent hole transfer through the xylyl bridge to the TPA inhibited recombination with the injected electron. Interestingly, there was no kinetic advantage with respect to charge recombination for the phenyl-bridged compounds.[32] To minimize free energy losses associated with the hole transfer reaction, the Ru$^{III/II}$ and TPA$^{+/0}$ reduction potentials were nearly the same, and for these compounds, $|E_{1/2}(Ru^{III/II}) - E_{1/2}(TPA^{+/0})| \leq 180$ mV. Upon one-electron oxidation of Ru^{II}, electron transfer originated from TPA. However, the opposite was true when TPA$^+$ was electrochemically generated prior to Ru^{II} oxidation, Scheme 1. Hence, the experimental approach used herein allowed optical electron transfer to be explored in opposite directions through the same bridge.

One would reasonably expect similar low-energy IVCT transitions regardless of the direction for symmetric compounds. Indeed, the most striking observation in the absorption spectra of the mixed-valent compounds was the appearance of a low-energy IVCT transition, $\lambda_{max} \sim 1000$ nm for Ru^{II}–B–TPA$^+$ (**2p$_C$/nITO**), that was substantially less pronounced for the opposite mixed-valent state, Ru^{III}–B–TPA (**1p$_C$/nITO**). Instead, the mixed-valent form of **1p$_C$/nITO** displayed an intense absorption near 480 nm. However, the absorption spectra of the ground- and fully oxidized states were nearly identical spectroscopically. A low-energy IVCT transition is characteristic of *direct* electron transfer between the two redox active sites.[27] In contrast, the higher energy visible absorption band is most consistent with TPA to cyclometalating ligand charge transfer.[42,43] Here, the optical excitation proceeds from TPA-centered orbitals to an unoccupied high energy cyclometalating ligand orbital, implying *indirect* charge transfer. A depiction of the alternative pathways is provided in Scheme 2. An important point arises in distinguishing "direct" and "indirect" pathways which correspond to optical charge-transfer transitions rather than thermal electron-transfer reactions. Regardless, analysis of the mixed-valent absorptions with a two-state model provided very different electronic coupling parameters, as discussed further below.

To further understand the influence of different optical pathways on the electronic coupling, a common two-state model was utilized to characterize the electronic coupling, H_{DA}, between Ru^{II} and TPA. The analysis indicated that H_{DA} was significantly different between these two discrete pathways. That is, that the electronic coupling seemed to depend on the electron-transfer direction due to changes in the orbitals accessed during light absorption.

In addition to the two-state model, a three-state superexchange model was also used. This model partitions the *direct* coupling between Ru^{II} and TPA, H_{DA}, into stepwise electronic coupling elements between the Ru^{II} and bridge (H_{AB}) as well as the TPA and the bridge (H_{DB}), Scheme 2. The three-state superexchange analysis revealed that the Ru^{II}/TPA coupling was pathway independent. Remarkably, even though the orbitals accessed during the optical charge transfer were found to ultimately depend on the electron-transfer direction, H_{DA} was found to be independent of the direction. Evidence of these pathways and the electronic couplings responsible for them are described further below beginning first with the electrochemical properties of the compounds.

Electrochemistry. Figure 6 provides a visual representation of the reduction potentials determined from spectroelectrochemical experiments. The Ru$^{III/II}$ reduction potentials were significantly (~100 mV) more negative when anchored to the oxide surface than in fluid solution. Such behavior has previously been reported and emanates from the inductive influence of the electron withdrawing ester groups relative to

DOI: 10.1021/jacs.8b02715
J. Am. Chem. Soc. 2018, 140, 7176–7186

Scheme 2. Representation of Superexchange Theory for Bridge-Mediated Electron Transfer[a]

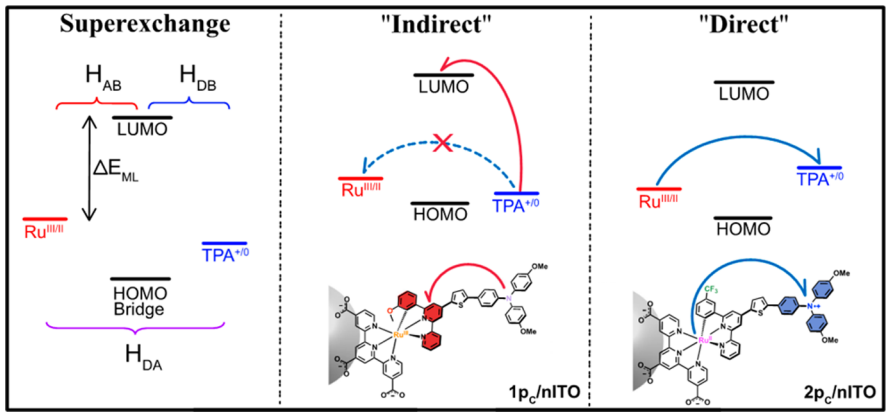

[a]'Indirect' electron transfer upon Ru^{II} oxidation (middle) and 'direct' electron transfer upon TPA oxidation (right).

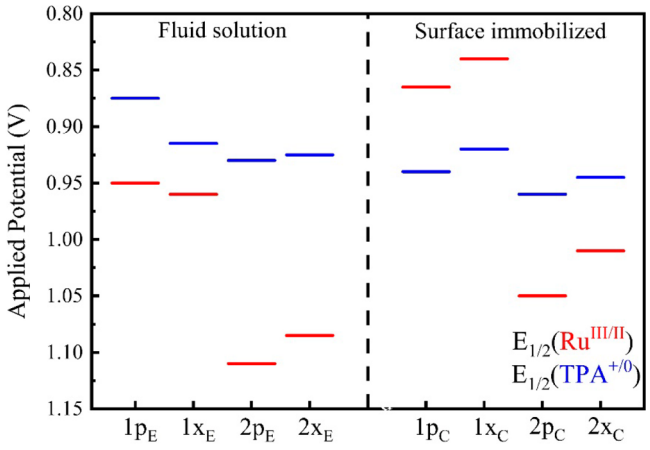

Figure 6. Representation of $E_{1/2}(Ru^{III/II})$ (red) and $E_{1/2}(TPA^{+/0})$ (blue) for the eight compounds in fluid acetonitrile solution and immobilized nITO.

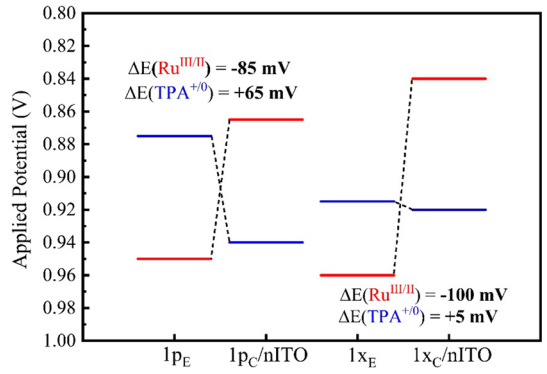

Figure 7. Redox potential switch upon surface immobilization for $\mathbf{1p_E}$ and $\mathbf{1p_C/nITO}$ as well as $\mathbf{1x_E}$ and $\mathbf{1x_C/nITO}$. The dashed lines connecting the redox potentials are guides to the eye.

the carboxylates present on the oxide surface.[38] Interestingly, the $E_{1/2}(TPA^{+/0})$ potentials were nearly insensitive to substituents on the terpyridine ligand, while the phenyl-bridged compounds showed a marked 75 mV positive shift. Such behavior is consistent with a through-bond inductive effect transmitted through the conjugated phenyl-bridge.

An important lesson from these comparative studies is that the surface anchoring groups can in themselves alter interfacial energetics. A clear example is $\mathbf{1p_E}$, where the TPA was oxidized first in solution while the Ru^{II} is oxidized first when anchored to the oxide, Figure 7. Such a redox "switch" would not have been recognized if the solution behavior of the ester (and presumably the carboxylic acid) were assumed to be the same as that for the carboxylate form present on the oxide surface.

A more subtle influence of the oxide surface was found in the non-Nernstian redox chemistry. In prior studies on TiO_2, it was found that a much larger potential step was required to induce a factor of 10 change in concentration of the Ru^{III} /Ru^{II} ratio relative to that for TPA^+/TPA.[39] Both required more than the 59 mV predicted by the Nernst equation for a one-electron-transfer process at room temperature. This behavior was attributed to an electric field effect wherein charges at the oxide interface create fields that influence the proximate Ru^{II} center to a greater degree than the more distant TPA.[44,45] Similar effects of this type have been demonstrated for porphyrazines immobilized onto gold, where the first reduction potential was increased by ~ +400 mV based on proximity to the surface.[46] The present case was attributed to an electric field effect, rather than an inductive effect, as the non-ideality factor was insensitive to the coupling provided by the bridging ligand.[47] Small, but measurable, deviations from Nernstian behavior were quantified for the ester derivatives in fluid acetonitrile electrolyte. The origin(s) of this behavior is(are) less clear yet may result from ion-pairing interactions in the electrolyte that will be the subject of future research.

Mulliken Hush H_{DA} Calculations. The IVCT absorption band has traditionally been used to determine the strength of orbital interactions between the "donor" and "acceptor" potential energy surfaces along a reaction coordinate. The magnitude of H_{DA} was calculated using the semi-classical theory of Mulliken and Hush, eq 3. Here the macroscopic parameters of the IVCT transition, namely the full-width at half-max $\Delta\nu_{1/2}$ (cm^{-1}), molar absorption coefficient at the absorbance maximum, ε_{max}, transition energy E_{op} (cm^{-1}), as well as the distance between centers, r (Å), allows for direct calculation of coupling matrix elements.[48] Spectral deconvolution and subsequent least-squares analysis with multiple Gaussian functions afforded band parameters and successfully minimized the influence of overlapping absorption bands that would otherwise have overestimated the fwhm and ε_{max} values of the IVCT transition.

DOI: 10.1021/jacs.8b02715
J. Am. Chem. Soc. 2018, 140, 7176−7186

$$H_{DA} = \frac{0.0206}{r}\sqrt{E_{op}\varepsilon_{max}\Delta\nu_{1/2}} \quad (3)$$

Constructing one-dimensional approximations of the potential energy surfaces for the product and reactant states presents a powerful tool to visualize electronic transitions arising as a result of mixed-valent redox states. Scheme 3 represents a three-state model, discussed in more detail below, and represents the reactant (blue), product (red), and bridge (green) states in the absence (dashed) and presence (solid) of electronic coupling, H_{DA}.[42] Experimentally, $E_{op} = \Delta G^{\circ} + \lambda$, where ΔG° is the standard free energy change and λ is the reorganization energy. Unlike the two-state model, where the splitting between the product and reactants surfaces is $2H_{DA}$, in a three-state model this difference corresponds to H_{DA}. Energetically high-lying bridge states can often mediate electronic coupling between the energy surfaces as evidenced by intense donor-bridge charge-transfer transitions, with electronic coupling H_{DB}.

Scheme 3. Potential Energy Surface Diagram for Three-State Optical Electron Transfer[a]

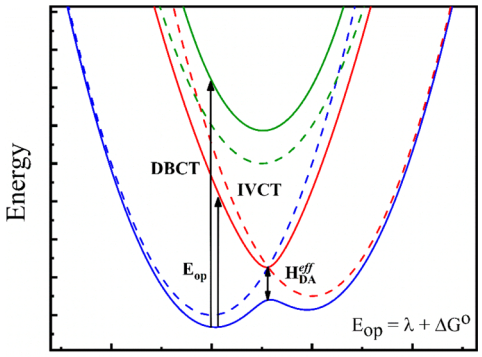

[a]DBCT (donor-to-bridge charge transfer) corresponds to the high energy TPA → ligand or generic metal-to-ligand charge transfer transition. IVCT (intervalence charge transfer) corresponds to a low energy transition between TPA and Ru^{III}. Effective coupling, H_{DA}^{eff} arises from mixing between all three surfaces, which enables the optical transitions to be observed.

The calculation of H_{DA} by eq 3 requires an estimate of the charge-transfer distance, r, which was assumed to be the geometric distance between the Ru^{II} metal center and central nitrogen atom of the TPA group. Electronic coupling calculated by this method presents a lower-limit.[49−51] A distance of 14 and 13 Å for "direct" and "indirect" electron transfer was garnered from density functional theory optimized structures, respectively.

These analyses yielded values of H_{DA} on the order of 950 cm^{-1} for **2p$_C$/nITO**. In the case of **1p$_C$/nITO**, the higher energy IVCT type band gave $H_{DB} \sim 2500$ cm^{-1}. We emphasize that the calculated coupling for **1p$_C$/nITO** represents TPA to cyclometalating ligand coupling, Scheme 2. A crude estimate of H_{DA} was possible for the low energy transition observed in the mixed-valent spectrum **1p$_C$/nITO** in the near-IR, $\varepsilon_{max} \sim 1300$ M^{-1} cm^{-1}, and gave $H_{DA} \leq 250$ cm^{-1}. As a control experiment, the magnitude of H_{DA} was determined in a similar way for the compounds in fluid solution by oxidation with $Cu(ClO_4)_2$ and are presented in Table 2 with spectra provided in Figure 8. Both **1p$_E$** and **2p$_E$** had spectral signatures similar to that of **2p$_C$/nITO** with IVCT bands appearing ~1000 nm, with $H_{DA} \approx 950$ cm^{-1}. By contrast, the **x-series** compounds did not display any indication of IVCT transitions at concentrations used herein, and H_{DA} was estimated to be <100 cm^{-1}.[32] Additionally, while K_c values have been reported to correlate strongly with electronic coupling, careful analysis has provided evidence that this approach is not always applicable.[52,53]

Table 2. Tabulated Values of IVCT Band Parameters and the Associated Electronic Coupling Matrix Elements

compd	E_{QP} (nm) ($\varepsilon \times 10^3$ M^{-1} cm^{-1})[b]	$\Delta\nu_{1/2}$ (cm^{-1})[e]	H_{DA} (cm^{-1})[e]	H_{DB} (cm^{-1})
1p$_E$[a]	1025 (9.0)	4480	920[c]	
2p$_E$[a]	1000 (11.4)	4080	1000[c]	
1p$_C$/nITO	480 (29.8)	4000		2500[d]
2p$_C$/nITO	1110 (10.5)	4460	950[c]	

[a]Measured by chemical oxidation with Cu(II). [b]Determined from spectral modeling after correcting for comproportionation. [c]Calculated for direct IVCT from the low-energy bands. [d]Electronic coupling between the TPA center and the cyclometalating ligand, H_{DB}. [e]From deconvoluted spectral analysis.

The calculated electronic coupling values presented in Table 2 for phenyl-bridged compounds that undergo direct ET are among the highest reported for this class of compounds.[54−56] It is worthwhile to place the studied compounds in the context of other bis-tridentate Ru^{II} compounds with similar cyclometalating motifs to briefly address what factors contribute to the strong electronic interactions. Sauvage and others have shown that electronic coupling between centers was enhanced when the N atom of the central pyridine ring in 2,2′,2″-terpyridine was replaced with a carbon atom, Scheme 4.[57−59] However, when a *peripheral* nitrogen was replaced with a carbon atom, there was no evidence for coupling between the metal centers. Other investigations of Ru^{II}−B−TPA compounds, where B = phenyl, has also shown appreciable coupling on the order of $H_{DA} \sim 450$ cm^{-1}.[60,61] In this regard, it is surprising that electronic coupling is strong in the present compounds, $H_{DA} \sim 1000$ cm^{-1}, considering that the Ru−C bond is in a peripheral position. This highlights the importance of the thiophene moiety as an effective mediator of electronic coupling, which has recently garnered much experimental interest.[35,62−64]

Superexchange H_{DA} Calculations. The McConnell relationship for superexchange has been widely invoked for many cases of long-range electron transfer where the redox orbitals are degenerate in energy; an energetic situation that holds approximately for these compounds.[65,66] When ET is mediated by the high-lying bridge LUMO transiently, the electronic coupling, H_{DA}, can be calculated through eq 4 as derived by Ratner and co-workers.[67,68]

$$H_{DA} = \frac{H_{DB}H_{AB}}{E - E_B} \quad (4)$$

This expression treats the electronic coupling between the donor and acceptor sites as the product of multi-site, or stepwise, electronic coupling elements between the donor and the bridge, H_{DB}, and between the bridge and the acceptor, H_{BA}.[69,70] The quantity $E - E_B$ corresponds to the energy separation between the donor or acceptor, E, and the bridging ligand, E_B, and is frequently referred to as the tunneling energy gap.[71−73] It is difficult to measure experimentally but can be

DOI: 10.1021/jacs.8b02715
J. Am. Chem. Soc. 2018, 140, 7176−7186

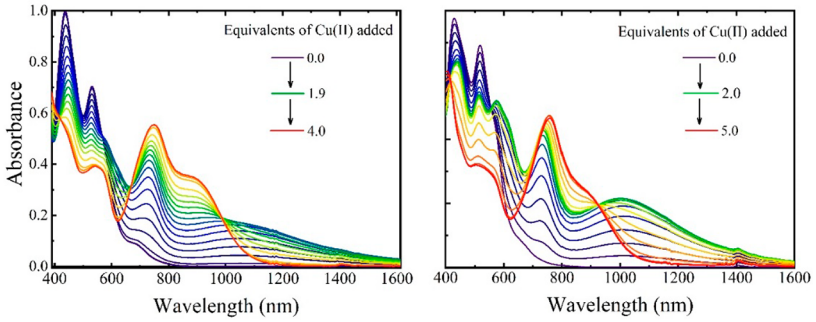

Figure 8. UV−vis−NIR absorption spectra of $\mathbf{1p_E}$ (left) and $\mathbf{2p_E}$ (right) in neat CH_3CN with Cu(II) titrated in as a chemical oxidant. Note the appearance of low energy IVCT transitions at ∼1000 nm for both compounds.

Scheme 4. Previously Reported Cyclometalated Ru^{II} Mixed-Valent Compounds with the Corresponding Values of H_{DA}[a]

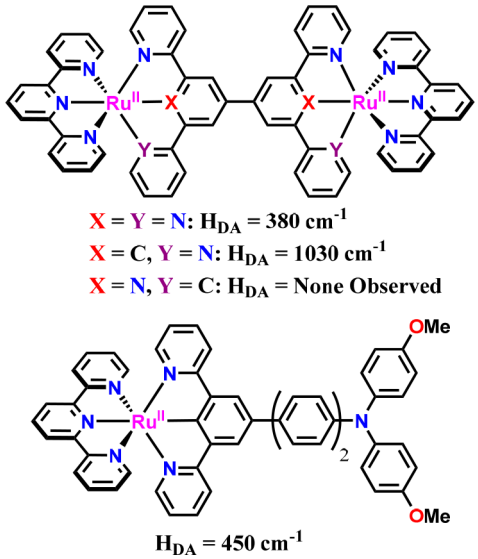

[a]Taken from refs 46−48 and 52.

related to the redox potentials of the individual donor, bridge, and acceptor units.[74]

For optical investigations of moderately coupled mixed-valent charge transfer compounds where the bridge orbitals mediate ET, the Creutz, Newton, and Sutin model depicted in Scheme 3 provides the *effective* coupling through eq 5.[48] The same methodology was used for the phenyl bridged compounds studied herein.

$$H_{DA}^{eff} = \frac{H_{DB}H_{AB}}{2\Delta E_{ML}} \quad (5)$$

In this expression, the term ΔE_{ML} refers to the difference between the metal and bridge states and is given by eq 6,

$$\frac{1}{\Delta E_{ML}} = \frac{1}{2}\left(\frac{1}{\Delta E_{MLCT}} + \frac{1}{\Delta E_{MLCT} - \Delta E_{IVCT}}\right) \quad (6)$$

where ΔE_{MLCT} and ΔE_{IVCT} are the spectroscopically observed energies for the metal to cyclometalating ligand transition and the IVCT transition, respectively.[26] Similar approaches often approximate this factor as differences in free energy or ionization potentials.[75,76] Unfortunately, the measurement of electrochemical redox potentials of cyclometalating ligands often result in irreversible electrochemistry. Onset reduction potentials typically begin at −1.9 V vs NHE.[36,77] Note the factor of 2 in eq 6 arises from a degeneracy factor for symmetric compounds and is not necessary in this analysis.

The value of ΔE_{IVCT} is readily available from the compounds that exhibit direct IVCT and is $\sim 10^3$ cm^{-1}. Inspection of the ground-state UV−vis spectra provides the value of ΔE_{MLCT} for Ru to the cyclometalating ligand, $\lambda_{max} = 23.5 \times 10^3$ cm^{-1} (425 nm), which was observed at higher energy relative to the Ru^{II} to terpyridine MLCT, ∼520 nm, presumably due to the electron rich nature of the covalent Ru−C bond.[29] From these values, ΔE_{ML} was found to be 2.2 eV. Electronic coupling between the metal and the ligand, H_{AB}, was calculated from eq 5 with typical line widths for polypyridyl MLCT transitions, $\Delta\upsilon_{1/2} = 4000$ cm^{-1}, and common values for metal−ligand coupling values, H_{AB}, range from 3 to 6×10^3 cm^{-1} for Ru^{II} to bipyridyl MLCT transitions.[48] This analysis provided $H_{AB} = 8400$ cm^{-1}; such a large degree of coupling is startling but is not unreasonable considering that strong σ-donating and π-back bonding effects are operative for a covalent Ru−C bond. The magnitude of H_{DB} is provided in Table 2 for $\mathbf{1p_C/nITO}$.

With all of the necessary quantities in hand, the effective coupling for TPA → Ru^{III} ET was calculated, $H_{DA}^{eff} = 1200$ cm^{-1}, which is likely an upper limit for the coupling arising from underestimating ΔE_{ML} and/or overestimating H_{AB}. However, the value calculated here is consistent with the results of Creutz, Newton, and Sutin.[48] A critical experimental detail that indicates an alternative optical pathway may be operative is the absence of an appreciable low energy transition for $\mathbf{1p_C/nITO}$ relative to $\mathbf{2p_C/nITO}$, Figure 5. Indeed, since the coupling is large, $H_{DA}^{eff} = 1200$ cm^{-1}, then the appearance of a low-energy transition would be expected under the experimental conditions. Phrased differently, this raises an interesting question: Why is a low-energy transition absent in $\mathbf{1p_C/nITO}$ despite having a comparable effective electronic coupling? This is likely the result of the alternative orbital pathway that proceeds virtually through the ligand LUMO in superexchange interaction.

In addressing the alternative pathway it is likely that the bridge previously defined as phenyl-thiophene is influenced by the electron-donating/-withdrawing ability of the $-OCH_3$ or $-CF_3$ substituents on the cyclometalating ring. Qualitatively, one would expect the donating nature of the $-OCH_3$ to destabilize the bridge LUMO relative to $-CF_3$.[78] Therefore, the tunneling energy gap ($E - E_b$, eq 3) should be larger for $\mathbf{1p_C/nITO}$, and thus, less contribution from a superexchange pathway would be expected. This is contrary to experiment where the indirect path was operative for electron transfer.

DOI: 10.1021/jacs.8b02715
J. Am. Chem. Soc. 2018, 140, 7176−7186

Therefore, it seems that inductive effect of the two groups does not appear to be significant.

From this analysis, an important distinction exists for optical versus thermal electron transfer. In thermal electron-transfer processes, the tunneling energy gap represents the energetic difference between the donor or acceptor orbitals and the bridge HOMO or LUMO at the transition state of the reaction.[79] On the other hand, mixing between states during optical ET necessarily occurs between high-lying unoccupied bridge orbitals while the system is in the nuclear geometry of the ground state. In principle, the bridge-centered HOMO also contributes to the total superexchange interaction, though it is difficult to quantify the impact without spectroscopic handles such as ligand to metal charge-transfer transitions.[70] Indeed, cyclometalation of the Ru^{II} center moves the energy of the bridge HOMO closer to that of the $Ru^{III/II}$ state, which provides access to more energetically favorable thermal pathways whereas for optical transitions a LUMO-mediated superexchange mechanism is most prominent.[32,56,80] Thus, thermal and optical electron transfer occur through very different mechanisms.

CONCLUSION

The electrochemical redox potentials and spectroscopic features of eight cyclometalated Ru^{II} compounds immobilized on a surface and in fluid solution were reported. Electrochemical experiments indicated that ΔG° between the two centers was small enough to enable interchange of the molecular HOMO between Ru^{II} and TPA. Upon one-electron oxidation, appreciable amounts of the mixed-valent state were formed. Compounds containing a phenyl bridge displayed intense IVCT transitions that were absent for the xylyl-bridged compounds. The electronic coupling between the Ru^{II} and TPA redox active centers was determined using a combination of Mulliken−Hush and a three-state superexchange-type analysis.

This analysis indicated that modifying the direction of electron transfer in model donor−bridge−acceptor compounds with an identical molecular bridge can provide access to different orbital transitions that may facilitate electron transfer. Such orbital pathways are evident in the steady-state electronic spectra of the one-electron oxidized forms of the conjugated phenyl-bridged compounds. Intense IVCT transitions provided direct approaches to measuring and characterizing the electronic coupling between the Ru^{II} and TPA redox centers. Use of a two-state model indicated that the electronic coupling between the Ru^{II} and TPA centers ultimately depended on the direction, i.e., what orbitals the transition originated from. However, the use of a three-state model indicated that electronic coupling was independent of the charge-transfer direction.

The origins of the different spectral features can be qualitatively understood through the molecular orbitals and electron densities. Each redox state possesses significantly different orbital character between the Ru^{II} d-orbitals and nitrogen sp^3 orbitals. To a first approximation, the Ru^{II} dπ orbitals mix significantly with the cyclometalating ligand π^* orbitals and this degree of mixing is expected to decrease dramatically when the Ru^{II} is oxidized to Ru^{III}. By comparison, the amine orbitals are not as diffuse and upon oxidation of TPA, direct charge transfer from Ru^{II} occurs to the empty orbitals of the TPA unit because of the large electron density associated with the Ru^{II} and the corresponding cyclometalating ligand states. In the opposite case, the absence of electron density in the Ru^{III} dπ orbitals cannot be accessed directly by the TPA electron density, which results in a charge transfer pathway that more easily proceeds from the amine to the cyclometalating ligand proximal to the Ru^{III} center.

A systematic study of eight Ru^{II}−B−TPA compounds both in solution and anchored onto a conductive surface was carried out. Spectroscopic and electrochemical experiments revealed that, following one-electron oxidation, charge transfer proceeded in different directions across a common bridge. This study demonstrated that electronic coupling between the two redox active centers is independent of which center is oxidized first. This was accomplished through explicit inclusion of high energy bridge-centered orbitals. Taken together, these observations present a fundamental contribution to the study of hybrid inorganic/organic materials that have potential applications in energy conversion or storage or as electrochromic materials.

EXPERIMENTAL SECTION

Thin Films and Sensitization. Colloidal nITO was prepared by previously published literature methods and deposited onto 1 cm wide optically transparent F-doped SnO_2 glass slides via doctor blading. The resulting films were usually 3 μm thick. The newly deposited films were annealed following the procedure of Farnum et al. to yield oxidized nITO, which appeared pale yellow to the unaided eye.[81] Films were sensitized by immersion in stock solutions of a carboxylate derivative of one of the compounds in neat methanol for 10−20 min. The resulting thin films had peak absorbance values of 0.6 or lower in their electronic ground states over the range of wavelengths measured.

Spectroscopic Characterization. UV−vis absorption spectra were measured using a Varian Cary 60 spectrometer in a 1 cm path length cuvette. The molar extinction coefficients for the ester derivatives were determined in neat acetonitrile. However, the carboxylic acid derivatives were not soluble in acetonitrile and only sparingly soluble in neat methanol. To completely dissolve the compounds, 1 equivalent of ∼1.5 M tetrabutylammonium hydroxide (TBAOH) in water was added to the methanol solution. In a typical experiment, stock solutions of 25 mL were prepared with 1 equiv of base which was approximately 0.5 μL of the stock TBAOH solution, except for $\mathbf{1p}_{C}$, which required 5 μL. The resulting change in volume was considered negligible.

Solution Spectroelectrochemistry. Formal reduction potentials in bulk solution were determined in CH_3CN containing 100 mM $LiClO_4$ as the supporting electrolyte in a standard three-electrode setup. The working electrode was a Pt honeycomb microelectrode with a Pt counter (Pine Research Instruments) and a nonaqueous pseudo-Ag/AgCl reference electrode. The half-wave potential of the ferrocene redox couple ($Fc^{+/0}$) was measured in 100 mM $LiClO_4$ in CH_3CN both before and after the experiment to account for potential drift. The pseudoreference electrode was externally referenced to NHE by using the measured value of the Fc(+/0) redox couple and adding a standard value of +630 mV.[82] Spectra were collected using a Avantes AvaLight DHc light source with an Avantes StarLine AvaSpec-2048 UV/vis spectrometer, while the electrochemical potential was applied using a Pine Wavenow potentiostat. All of the devices were controlled by Aftermath software (Pine Research Instruments).

The resulting potential-dependent spectra were analyzed by subtracting the ground-state spectrum of the molecule at each applied potential, resulting in so-called "difference spectra". The difference spectra, which represented changes due to the applied potentials, displayed positive values of absorbance indicative of feature growth and negative values of absorbance which indicate ground-state bleaching. Single-wavelength data were selected at maxima of growths and bleaches, isosbestic points, and intermediate wavelengths and fit to the Nernst equation to give the formal reduction potential of each oxidation event.

Surface Spectroelectrochemistry. UV/vis/NIR spectroelectrochemistry of the carboxylate-substituted molecules anchored onto thin

DOI: 10.1021/jacs.8b02715
J. Am. Chem. Soc. 2018, 140, 7176−7186

films of nITO on FTO slides were monitored using a Varian Cary 5000 spectrometer while simultaneously applying a potential. The slides were immersed in 100 mM $LiClO_4/CH_3CN$ solutions at a 45° angle in a 1 cm path length cuvette at low surface coverages. Electrochemical potentials were applied by a BASi epsilon potentiostat using the EClipse software in a standard 3-electrode arrangement. In the experiments, the FTO glass served as the working electrode with a Pt gauze counter and a Ag/AgCl pseudoreference electrode. Potentials were applied stepwise on the order of 10−20 mV/step and held for a minimum of 15 s before a scan was taken to ensure electrochemical equilibrium, after which data were recorded. Spectra were recorded until changes were minimized. The same methodology to standardize the applied potentials was used as previously stated. The Cary 5000 was operated in the standard dual beam set up with reduced slit height, fixed slit-band widths, and a grating and detector changeover at 850 nm. Notably, a "spectral discontinuity" was occasionally observed during the experiment, which is not uncommon, and was corrected for by adjusting the appropriate slit-band widths. Background spectra collected from 350 nm to a minimum of 1700 nm were of bare FTO and solvent to account for the NIR absorbance of CH_3CN. Measuring beyond 2000 nm was not possible due to intense cuvette absorption. Separate background spectra of nITO were recorded due to its behavior as a function of applied bias.

Chemical Oxidation. Redox titrations of $\mathbf{1p_E}$ and $\mathbf{2p_E}$ were performed on ester derivatives in neat acetonitrile using $Cu(ClO_4)_2 \cdot 6H_2O$ as the sacrificial oxidant in the form of the Cu(II/I) redox couple.[83,84] In all experiments, a stock solution of 0.6 mM $Cu(ClO_4)_2$ was used. Aliquots of 20 μL were added to a 1 cm path length cuvette containing 3.0 mL of ∼1 μM ester compound with a Hamilton syringe and carefully stirred to ensure equilibrium was established. Spectra were recorded using a Varian Cary 5000 spectrometer, in a similar fashion described as above, until subsequent spectral changes were negligible. The resulting spectra were corrected as a function of total volume over the course of the titration.

■ ASSOCIATED CONTENT

Supporting Information

The Supporting Information is available free of charge on the ACS Publications website at DOI: 10.1021/jacs.8b02715.

Experimental details of spectral modeling and reconstruction, information about the comproportionation, and chemical oxidation (PDF)

■ AUTHOR INFORMATION

Corresponding Author

*gjmeyer@email.unc.edu

ORCID

Ludovic Troian-Gautier: 0000-0002-7690-1361
Renato N. Sampaio: 0000-0002-7158-6470
Curtis P. Berlinguette: 0000-0001-6875-849X
Gerald J. Meyer: 0000-0002-4227-6393

Notes

The authors declare no competing financial interest.

■ ACKNOWLEDGMENTS

This material is based upon work solely supported as part of the UNC EFRC: Center for Solar Fuels, an Energy Frontier Research Center funded by the U.S. Department of Energy, Office of Science, Office of Basic Energy Sciences under Award No. DE-SC0001011. L.T.-G. acknowledges personal fellowships from the Belgian American Educational Foundation (BAEF) as well as the Bourse d'Excellence Wallonie-Bruxelles (WBI.World). The authors thank Tyler C. Motley for helpful discussions.

■ REFERENCES

(1) Mas-Torrent, M.; Rovira, C.; Veciana, J. *Adv. Mater.* **2013**, *25*, 462−468.
(2) Mortimer, R. J. *Chem. Soc. Rev.* **1997**, *26*, 147−156.
(3) Browne, W. R.; Feringa, B. L. *Annu. Rev. Phys. Chem.* **2009**, *60*, 407−428.
(4) Wu, Z.; Cui, P.; Zhang, G.; Luo, Y.; Jiang, J. *J. Phys. Chem. Lett.* **2018**, *9*, 837−843.
(5) He, B.; Wenger, O. S. *J. Am. Chem. Soc.* **2011**, *133*, 17027−17036.
(6) Murase, R.; Leong, C. F.; D'Alessandro, D. M. *Inorg. Chem.* **2017**, *56*, 14373−14382.
(7) Magri, D. C.; Brown, G. J.; McClean, G. D.; de Silva, A. P. *J. Am. Chem. Soc.* **2006**, *128*, 4950−4951.
(8) de Silva, A. P.; Gunaratne, H. Q. N.; McCoy, C. P. *J. Am. Chem. Soc.* **1997**, *119*, 7891−7892.
(9) Cui, B.-B.; Zhong, Y.-W.; Yao, J. *J. Am. Chem. Soc.* **2015**, *137*, 4058−4061.
(10) Chen, H.-Y.; Ardo, S. *Nat. Chem.* **2017**, *10*, 17−23.
(11) Troian-Gautier, L.; DiMarco, B. N.; Sampaio, R. N.; Marquard, S. L.; Meyer, G. J. *J. Am. Chem. Soc.* **2018**, *140*, 3019−3029.
(12) Khoudiakov, M.; Parise, A. R.; Brunschwig, B. S. *J. Am. Chem. Soc.* **2003**, *125*, 4637−4642.
(13) Yang, M.; Thompson, D. W.; Meyer, G. J. *Inorg. Chem.* **2002**, *41*, 1254−1262.
(14) Alibabaei, L.; Brennaman, M. K.; Norris, M. R.; Kalanyan, B.; Song, W.; Losego, M. D.; Concepcion, J. J.; Binstead, R. A.; Parsons, G. N.; Meyer, T. J. *Proc. Natl. Acad. Sci. U. S. A.* **2013**, *110*, 20008−20013.
(15) Robson, K. C. D.; Koivisto, B. D.; Gordon, T. J.; Baumgartner, T.; Berlinguette, C. P. *Inorg. Chem.* **2010**, *49*, 5335−5337.
(16) Kreitner, C.; Mengel, A. K. C.; Lee, T. K.; Cho, W.; Char, K.; Kang, Y. S.; Heinze, K. *Chem. - Eur. J.* **2016**, *22*, 8915−8928.
(17) Ding, Y.; Jiang, Y.; Zhang, W.; Zhang, L.; Lu, X.; Wang, Q.; Zhou, G.; Liu, J.-m.; Kempa, K.; Gao, J. *J. Phys. Chem. C* **2017**, *121*, 16731−16738.
(18) Spettel, K. E.; Damrauer, N. H. *J. Phys. Chem. C* **2016**, *120*, 10815−10829.
(19) Benniston, A. C.; Harriman, A. *Chem. Soc. Rev.* **2006**, *35*, 169−179.
(20) Kennedy, S. R.; Goyal, P.; Kozar, M. N.; Yennawar, H. P.; Hammes-Schiffer, S.; Lear, B. J. *Inorg. Chem.* **2016**, *55*, 1433−1445.
(21) Tang, J.-H.; Wu, S.-H.; Shao, J.-Y.; Nie, H.-J.; Zhong, Y.-W. *Organometallics* **2013**, *32*, 4564−4570.
(22) Harriman, A.; Heitz, V.; Sauvage, J. P. *J. Phys. Chem.* **1993**, *97*, 5940−5946.
(23) Cailliez, F.; Müller, P.; Firmino, T.; Pernot, P.; de la Lande, A. *J. Am. Chem. Soc.* **2016**, *138*, 1904−1915.
(24) Hush, N. S. In *Progress in Inorgic Chemistry*; John Wiley & Sons, Inc., 2007; pp 391−444.
(25) Creutz, C.; Taube, H. *J. Am. Chem. Soc.* **1969**, *91*, 3988−3989.
(26) Brunschwig, B. S.; Sutin, N. *Coord. Chem. Rev.* **1999**, *187*, 233−254.
(27) Brunschwig, B. S.; Creutz, C.; Sutin, N. *Chem. Soc. Rev.* **2002**, *31*, 168−184.
(28) Evans, C. E. B.; Naklicki, M. L.; Rezvani, A. R.; White, C. A.; Kondratiev, V. V.; Crutchley, R. J. *J. Am. Chem. Soc.* **1998**, *120*, 13096−13103.
(29) Robson, K. C. D.; Koivisto, B. D.; Yella, A.; Sporinova, B.; Nazeeruddin, M. K.; Baumgartner, T.; Grätzel, M.; Berlinguette, C. P. *Inorg. Chem.* **2011**, *50*, 5494−5508.
(30) Malagoli, M.; Brédas, J. L. *Chem. Phys. Lett.* **2000**, *327*, 13−17.
(31) Ellis, H.; Schmidt, I.; Hagfeldt, A.; Wittstock, G.; Boschloo, G. *J. Phys. Chem. C* **2015**, *119*, 21775−21783.
(32) Hu, K.; Blair, A. D.; Piechota, E. J.; Schauer, P. A.; Sampaio, R. N.; Parlane, F. G. L.; Meyer, G. J.; Berlinguette, C. P. *Nat. Chem.* **2016**, *8*, 853−859.
(33) Robson, K. C. D.; Sporinova, B.; Koivisto, B. D.; Schott, E.; Brown, D. G.; Berlinguette, C. P. *Inorg. Chem.* **2011**, *50*, 6019−6028.
(34) Kreitner, C.; Heinze, K. *Dalton Trans.* **2016**, *45*, 13631−13647.

DOI: 10.1021/jacs.8b02715
J. Am. Chem. Soc. 2018, 140, 7176−7186

(35) Koivisto, B. D.; Robson, K. C. D.; Berlinguette, C. P. *Inorg. Chem.* **2009**, *48*, 9644−9652.
(36) Wadman, S. H.; Lutz, M.; Tooke, D. M.; Spek, A. L.; Hartl, F.; Havenith, R. W. A.; van Klink, G. P. M.; van Koten, G. *Inorg. Chem.* **2009**, *48*, 1887−1900.
(37) Amthor, S.; Noller, B.; Lambert, C. *Chem. Phys.* **2005**, *316*, 141−152.
(38) Ardo, S.; Achey, D.; Morris, A. J.; Abrahamsson, M.; Meyer, G. J. *J. Am. Chem. Soc.* **2011**, *133*, 16572−16580.
(39) Hu, K.; Robson, K. C. D.; Beauvilliers, E. E.; Schott, E.; Zarate, X.; Arratia-Perez, R.; Berlinguette, C. P.; Meyer, G. J. *J. Am. Chem. Soc.* **2014**, *136*, 1034−1046.
(40) Sutton, J. E.; Sutton, P. M.; Taube, H. *Inorg. Chem.* **1979**, *18*, 1017−1021.
(41) D'Alessandro, D. M.; Keene, F. R. *Chem. Soc. Rev.* **2006**, *35*, 424−440.
(42) Kubiak, C. P. *Inorg. Chem.* **2013**, *52*, 5663−5676.
(43) Lambert, C.; Noll, G.; Schelter, J. *Nat. Mater.* **2002**, *1*, 69−73.
(44) Zaban, A.; Ferrere, S.; Gregg, B. A. *J. Phys. Chem. B* **1998**, *102*, 452−460.
(45) Yang, W.; Vlachopoulos, N.; Boschloo, G. *ACS Energy Letters* **2017**, *2*, 161−167.
(46) Vesper, B. J.; Salaita, K.; Zong, H.; Mirkin, C. A.; Barrett, A. G. M.; Hoffman, B. M. *J. Am. Chem. Soc.* **2004**, *126*, 16653−16658.
(47) Ardo, S.; Meyer, G. J. *J. Am. Chem. Soc.* **2011**, *133*, 15384−15396.
(48) Creutz, C.; Newton, M. D.; Sutin, N. *J. Photochem. Photobiol., A* **1994**, *82*, 47−59.
(49) Karki, L.; Lu, H. P.; Hupp, J. T. *J. Phys. Chem.* **1996**, *100*, 15637−15639.
(50) Cave, R. J.; Newton, M. D. *J. Chem. Phys.* **1997**, *106*, 9213−9226.
(51) Zheng, J.; Kang, Y. K.; Therien, M. J.; Beratan, D. N. *J. Am. Chem. Soc.* **2005**, *127*, 11303−11310.
(52) Winter, R. F. *Organometallics* **2014**, *33*, 4517−4536.
(53) D'Alessandro, D. M.; Keene, F. R. *Dalton Trans.* **2004**, 3950−3954.
(54) Zhong, Y.-W.; Gong, Z.-L.; Shao, J.-Y.; Yao, J. *Coord. Chem. Rev.* **2016**, *312*, 22−40.
(55) Shen, J.-J.; Shao, J.-Y.; Gong, Z.-L.; Zhong, Y.-W. *Inorg. Chem.* **2015**, *54*, 10776−10784.
(56) Shen, J.-J.; Zhong, Y.-W. *Sci. Rep.* **2015**, *5*, 13835−13843.
(57) Beley, M.; Collin, J. P.; Sauvage, J. P. *Inorg. Chem.* **1993**, *32*, 4539−4543.
(58) Patoux, C.; Launay, J.-P.; Beley, M.; Chodorowski-Kimmes, S.; Collin, J.-P.; James, S.; Sauvage, J.-P. *J. Am. Chem. Soc.* **1998**, *120*, 3717−3725.
(59) Barigelletti, F.; Flamigni, L.; Balzani, V.; Collin, J.-P.; Sauvage, J.-P.; Sour, A.; Constable, E. C.; Thompson, A. M. W. C. *J. Am. Chem. Soc.* **1994**, *116*, 7692−7699.
(60) Yao, C.-J.; Zhong, Y.-W.; Nie, H.-J.; Abruña, H. D.; Yao, J. *J. Am. Chem. Soc.* **2011**, *133*, 20720−20723.
(61) Yang, W.-W.; Zhong, Y.-W.; Yoshikawa, S.; Shao, J.-Y.; Masaoka, S.; Sakai, K.; Yao, J.; Haga, M.-a. *Inorg. Chem.* **2012**, *51*, 890−899.
(62) Jahnke, A. C.; Spulber, M.; Neuburger, M.; Palivan, C. G.; Wenger, O. S. *Chem. Commun.* **2014**, *50*, 10883−10886.
(63) Morseth, Z. A.; Pho, T. V.; Sheridan, M. V.; Meyer, T. J.; Schanze, K. S.; Reynolds, J. R.; Papanikolas, J. M. *ACS Appl. Mater. Interfaces* **2017**, *9*, 16651−16659.
(64) Cruz, C. D.; Christensen, P. R.; Chronister, E. L.; Casanova, D.; Wolf, M. O.; Bardeen, C. J. *J. Am. Chem. Soc.* **2015**, *137*, 12552−12564.
(65) McConnell, H. M. *J. Chem. Phys.* **1961**, *35*, 508−515.
(66) Lambert, C.; Risko, C.; Coropceanu, V.; Schelter, J.; Amthor, S.; Gruhn, N. E.; Durivage, J. C.; Brédas, J.-L. *J. Am. Chem. Soc.* **2005**, *127*, 8508−8516.
(67) Closs, G. L.; Miller, J. R. *Science* **1988**, *240*, 440−447.
(68) Ratner, M. A. *J. Phys. Chem.* **1990**, *94*, 4877−4883.
(69) Albinsson, B.; Mårtensson, J. *J. Photochem. Photobiol., C* **2008**, *9*, 138−155.
(70) Natali, M.; Campagna, S.; Scandola, F. *Chem. Soc. Rev.* **2014**, *43*, 4005−4018.
(71) Wenger, O. S.; Leigh, B. S.; Villahermosa, R. M.; Gray, H. B.; Winkler, J. R. *Science* **2005**, *307*, 99−102.
(72) Wenger, O. S. *Acc. Chem. Res.* **2011**, *44*, 25−35.
(73) Gray, H. B.; Winkler, J. R. *Proc. Natl. Acad. Sci. U. S. A.* **2005**, *102*, 3534−3539.
(74) Hankache, J.; Wenger, O. S. *Phys. Chem. Chem. Phys.* **2012**, *14*, 2685−2692.
(75) Lewis, F. D.; Liu, J.; Weigel, W.; Rettig, W.; Kurnikov, I. V.; Beratan, D. N. *Proc. Natl. Acad. Sci. U. S. A.* **2002**, *99*, 12536−12541.
(76) Hu, Y.; Mukamel, S. *Chem. Phys. Lett.* **1989**, *160*, 410−416.
(77) Kreitner, C.; Heinze, K. *Dalton Trans.* **2016**, *45*, 5640−5658.
(78) Schäfer, J.; Holzapfel, M.; Mladenova, B.; Kattnig, D.; Krummenacher, I.; Braunschweig, H.; Grampp, G.; Lambert, C. *J. Am. Chem. Soc.* **2017**, *139*, 6200−6209.
(79) Hupp, J. T.; Neyhart, G. A.; Meyer, T. J.; Kober, E. M. *J. Phys. Chem.* **1992**, *96*, 10820−10830.
(80) Constable, E. C.; Housecroft, C. E. *Polyhedron* **1990**, *9*, 1939−1947.
(81) Farnum, B. H.; Morseth, Z. A.; Brennaman, M. K.; Papanikolas, J. M.; Meyer, T. J. *J. Phys. Chem. B* **2015**, *119*, 7698−7711.
(82) Pavlishchuk, V. V.; Addison, A. W. *Inorg. Chim. Acta* **2000**, *298*, 97−102.
(83) Sreenath, K.; Suneesh, C. V.; Gopidas, K. R.; Flowers, R. A. *J. Phys. Chem. A* **2009**, *113*, 6477−6483.
(84) Quinton, C.; Alain-Rizzo, V.; Dumas-Verdes, C.; Clavier, G.; Miomandre, F.; Audebert, P. *Eur. J. Org. Chem.* **2012**, *2012*, 1394−1403.

DOI: 10.1021/jacs.8b02715
J. Am. Chem. Soc. 2018, 140, 7176−7186